Pseudoelasticity at Large Strains in Au Nanocrystals

X. Wendy Gu,[1,2,*] Lindsey A. Hanson,[3,4,*] Carissa N. Eisler,[4] Matthew A. Koc,[1] and A. Paul Alivisatos[1,4,5,6,†]
[1]*Department of Chemistry, University of California, Berkeley, Berkeley, California 94720, USA*
[2]*Department of Mechanical Engineering, Stanford University, Stanford, California 94305, USA*
[3]*Department of Chemistry, Trinity College, Hartford, Connecticut 06106, USA*
[4]*Materials Science Division, Lawrence Berkeley National Laboratory, Berkeley, California 94720, USA*
[5]*Department of Materials Science and Engineering, University of California, Berkeley, Berkeley, California 94720, USA*
[6]*Kavli Energy NanoScience Institute, University of California, Berkeley and Lawrence Berkeley National Laboratory, Berkeley, California 94720, USA*

(Received 5 March 2018; published 1 August 2018)

Pseudoelasticity in metals is typically associated with phase transformations (e.g., shape memory alloys) but has recently been observed in sub-10 nm Ag nanocrystals that rapidly recovered their original shape after deformation to large strains. The discovery of pseudoelasticity in nanoscale metals dramatically changes the current understanding of the properties of solids at the smallest length scales, and the motion of atoms at surfaces. Yet, it remains unclear whether pseudoelasticity exists in different metals and nanocrystal sizes. The challenge of observing deformation at atomistic to nanometer length scales has prevented a clear mechanistic understanding of nanoscale pseudoelasticity, although surface diffusion and dislocation-mediated processes have been proposed. We further the understanding of pseudoelasticity in nanoscale metals by using a diamond anvil cell to compress colloidal Au nanocrystals under quasihydrostatic and nonhydrostatic pressure conditions. Nanocrystal structural changes are measured using optical spectroscopy and transmission electron microscopy and modeled using electrodynamic theory. We find that 3.9 nm Au nanocrystals exhibit pseudoelastic shape recovery after deformation to large uniaxial strains of up to 20%, which is equivalent to an ellipsoid with an aspect ratio of 2. Nanocrystal absorbance efficiency does not recover after deformation, which indicates that crystalline defects may be trapped in the nanocrystals after deformation.

DOI: 10.1103/PhysRevLett.121.056102

Pseudoelasticity describes the reversible deformation of a material that is strained past its elastic limit, through a process in which atomic bonds are broken and reformed. Recently, rapid pseudoelastic recovery from large strains was observed in sub-10 nm Ag nanoparticles inside of a transmission electron microscope (TEM) [1]. The surprising observation of pseudoelasticity in Ag nanoparticles is diametrically opposed to the classical behavior of metals, in which irreversible plastic deformation occurs at large strains. This discovery adds to the growing body of evidence that strength, deformation, and defect dynamics in nanoscale solids cannot be extrapolated from the properties of their bulk counterparts. Pseudoelastic metallic nanostructures should have superior performance, including shape memory at low temperatures and the ability to rapidly heal from applied stresses. Pseudoelasticity in metal nanocrystals has been attributed to rapid surface diffusion [1,2], but defect-mediated processes such as the escape of dislocations through free surfaces [3,4] and the reversible passage of twin boundaries [5,6] are other possible mechanisms. Further insight into this phenomenon requires investigation of other nanocrystal sizes and metals at realistic temperatures and timescales, which can be challenging to achieve using *in situ* TEM or through atomistic modeling.

Here, 3.9 nm Au nanocrystals are compressed inside of a diamond anvil cell to determine whether deformation is reversible under volumetric and deviatoric strains. The outstanding physical properties of Au nanocrystals have enabled their widespread use in photonics [7,8], catalysis [9,10], sensing [11,12], and biomedical therapies [3,4]. The structural stability of Au nanocrystals is of interest for size and shape control during synthesis and fabrication [13,14], and the reliable operation of nanocrystal-based devices. Pseudoelasticity is expected in 3.9 nm nanocrystals according to the surface diffusion-based mechanism developed for Ag [1]. It is unclear whether pseudoelasticity will be observed in Au, which has slower atomic surface diffusion than Ag [15].

Diamond anvil cell compression has previously been used to study elastic properties and phase transformations in inorganic nanocrystals [16–21]. Nanocrystal structural changes are monitored *in situ* using optical absorption spectroscopy. Absorption spectroscopy reveals the localized surface plasmon resonance of the Au nanocrystals, which is generated by the resonant oscillation of conduction electrons

in response to light. The energy and intensity of the surface plasmon is highly sensitive to nanocrystal size and shape [22–24], and it can therefore be used to track deformation under pressure. The surface plasmon also depends on the density of crystalline defects in the nanocrystal [25,26], which is indicative of microstructural changes in the nanocrystals. We demonstrate the sensitivity of this detection method by using electrodynamics theory to model the optical response to shape and microstructural changes in the Au nanocrystals. It is found that subnanometer changes in nanocrystal aspect ratio lead to greater than 20 nm shifts in plasmon energy. Results from optical spectroscopy are corroborated using TEM. Using these techniques, we determine that Au nanocrystals rapidly recover their original shape after uniaxial deformation to large strains during single and multicycle loading inside of the diamond anvil cell. We believe that crystalline defects in the interior of the nanocrystal play a role in the pseudoelastic deformation based on an irreversible reduction in absorbance efficiency after pressurization.

Dodecanethiol-capped Au nanocrystals with diameters of 3.9 ± 0.9 nm were synthesized using organic-phase air-free techniques [Fig. 1(a)] [27]. Nanocrystals were transferred to the desired pressure medium and loaded into the diamond anvil cell for cyclic pressure testing. Ethylcyclohexane was used as a quasihydrostatic pressure medium, and toluene was used as a nonhydrostatic pressure medium [17,28]. Ruby fluorescence indicated that a quasihydrostatic pressure environment was maintained in ethylcyclohexane up to ~10 GPa, after which a slight deviation from hydrostatic pressure was observed (see the Supplementary Material [29]). Nanocrystal solutions were maintained in the dilute limit to ensure that optical changes are not due to particle-particle coupling. The refractive index of ethylcyclohexane increases by less than 0.006 RIU (refractive index unit) per gigapascal, while the refractive index of toluene and dodecanethiol (ligand shell) increases by 0.02 RIU per gigapascal (see the Supplemental Material [29]). Changes in path length and concentration during pressurization are accounted for by monitoring the cross-section area and height of the diamond anvil cell chamber (see the Supplemental Material [29]).

Figure 1(b) shows the extinction spectra of the Au nanocrystals under quasihydrostatic pressure up to 21 GPa. Extinction is dominated by absorption in nanocrystals that are much smaller than the wavelength of light [24], so extinction is referred to as absorbance from here on. The absorbance spectra change minimally under quasihydrostatic pressure. The plasmon peak wavelength (λ_{max}) increases by 5 nm as pressure is increased to 21 GPa (the spectral resolution is 2.7 nm), and it returns to the original plasmon wavelength as pressure is decreased to ambient conditions. The absorbance efficiency at the plasmon wavelength per volume of solution (Q_{max}) is determined at each pressure. By repeated measurements, it was found that the spectral resolution is 2.7 nm, the accuracy in absorbance efficiency is within 0.01, and uncertainty in pressure is ± 0.1 GPa. The change in Q_{max} from the first to the maximum pressure is within the measurement resolution, as is the change from the first to the last pressure (ambient pressure). Figure 1(c) shows the optical spectra of the Au nanocrystals under nonhydrostatic pressure up to 19 GPa. In contrast to the quasihydrostatic case, λ_{max} undergoes a large redshift as pressure is increased to 19 GPa, then returns to its original value after the pressure is removed. The shape of the optical spectrum at the end of the pressure cycle (ambient pressure) is similar to the initial spectrum, but Q_{max} is reduced at the end of the pressure cycle.

The changes in plasmon peak wavelength and absorbance efficiency under nonhydrostatic pressure are quantified in Fig. 2 for four experiments. Maximum pressures of 15 to 24 GPa were reached in these experiments, which resulted in a redshift in λ_{max} of 46 to 68 nm [Figs. 2(a)–2(d)]. The average optical shift is 3.2 nm per GPa. Upon removing the pressure, the final λ_{max} returned to within 0 to 8 nm of the initial λ_{max}. λ_{max} initially shifts rapidly at pressures below 3 GPa and then shifts more slowly at higher pressures

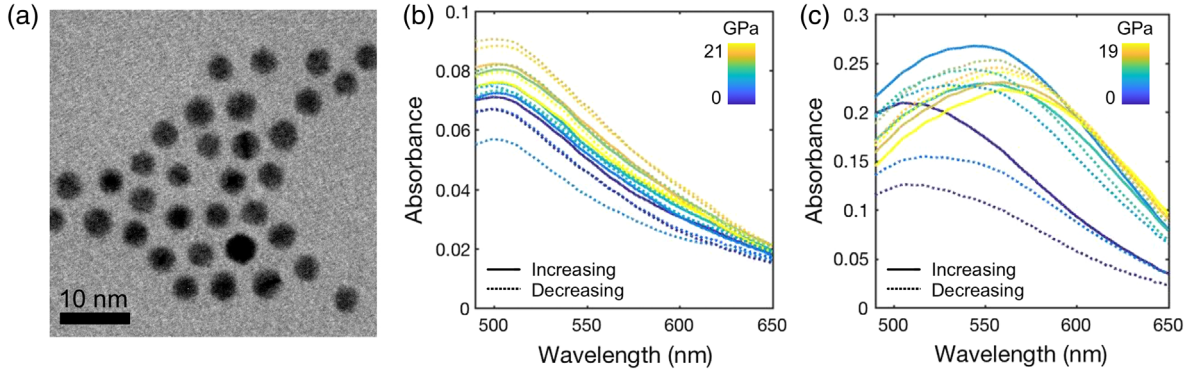

FIG. 1. High-pressure optical absorbance. (a) TEM image of 3.9 nm Au nanocrystals. Absorbance spectra in (b) quasihydrostatic pressure medium (ethylcyclohexane) and (c) nonhydrostatic pressure medium (toluene). Increasing pressures are solid lines, and decreasing pressures are dotted lines.

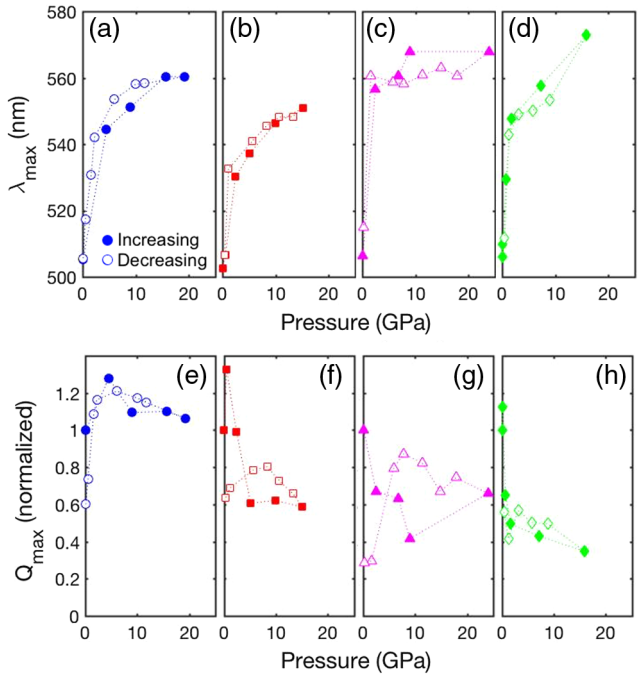

FIG. 2. Plasmon peak shifts in a nonhydrostatic pressure environment. (a)–(d) The plasmon peak wavelength (λ_{max}) and (e)–(h) the corresponding absorbance efficiency (Q_{max}) for four independent experiments. Q_{max} is normalized to Q_{max} at ambient pressure. Increasing pressures are filled symbols, and decreasing pressures are open symbols.

[Figs. 2(a)–2(d)]. The corresponding changes in Q_{max} are shown in Figs. 2(e)–2(h). The final absorbance efficiency is 30% to 60% of the initial absorbance efficiency. The changes in Q_{max} with pressure vary across the four experiments [Figs. 2(e)–2(h)]. In Fig. 2(e), Q_{max} is higher at elevated pressures. Figures 2(f) and 2(h) show an initial increase in Q_{max} at the first pressurized data point, and then a decrease in Q_{max} below the initial absorbance efficiency for subsequent pressures. Figure 2(g) shows an immediate decrease in Q_{max} with pressurization, and a Q_{max} that is lower than the initial Q_{max} for subsequent pressures. All experiments show hysteresis in Q_{max} between increasing and decreasing pressure.

The variation in the optical response across these experiments can be linked to differences in the magnitude of deviatoric pressure between experiments, and during the course of an experiment. The deviatoric strain across the sample chamber has been quantified by measuring the change in cross-section area and distance between the diamond platens for the experiments in Fig. 2, and it is observed to vary significantly between experiments (see the Supplemental Material [29]). Previous diamond anvil cell experiments on metallic powders under nonhydrostatic pressures have shown that uniaxial stress increases linearly with average pressure [40–42]; this is likely to occur during the experiments presented here as well.

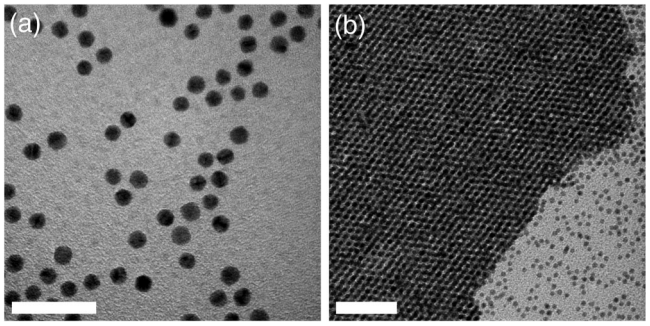

FIG. 3. TEM images of (a) individual (scale bar is 20 nm) and (b) self-assembled superlattice of Au nanocrystals after nonhydrostatic compression to 30 GPa (scale bar is 50 nm).

Spherical Au nanocrystals will become elongated spheroids under nonhydrostatic pressure. This change in nanocrystal shape is predicted to lead to a redshift in λ_{max} [22–24], which agrees well with our experimental observations. The reversibility of the observed redshift indicates that the nanocrystals return to their original shape when pressure is removed, which is quite surprising considering the large pressures involved. Further evidence of nanocrystal shape recovery is provided by postdeformation TEM images of the nanocrystals (Fig. 3). Nanocrystals were recovered after diamond anvil cell testing and dispersed onto a TEM grid. Postdeformation nanocrystals are very similar in appearance to as-synthesized nanocrystals: nanocrystals are spherical and contain crystalline domains after deformation (see the Supplemental Material [29]), and they are able to form close-packed three-dimensional assemblies upon slow drying [Fig. 3(b)]. Ordered nanocrystal assemblies can form only from highly monodisperse nanocrystals [43,44], which indicates that a large fraction of nanocrystals are spherical and reasonably monodisperse after deformation. These results do not explain the reduction in Q_{max} that results from the pressure cycle, which may be due to additional microstructural changes, like the creation of crystalline defects such as stacking faults, twin boundaries or stacking fault tetrahedra. Post-deformation TEM and optical microscopy images show that the nanocrystals do not agglomerate during the course of the pressure cycle (see the Supplemental Material [29]).

The source of the observed changes in λ_{max} and Q_{max} under pressure is investigated using optical modeling. A finite difference time domain model was used to calculate absorption of Au nanocrystals of different sizes and shapes, without accounting for compressional effects (e.g., changes in lattice parameter, electron density, or density of states). The size of the simulated nanocrystal was varied to explore the effect of volumetric strain on the optical response of Au nanocrystals under hydrostatic pressure [Fig. 4(a)]. Changes in refractive index during compression were accounted for in simulation. In agreement with the experimental observations, the simulated absorbance spectra do

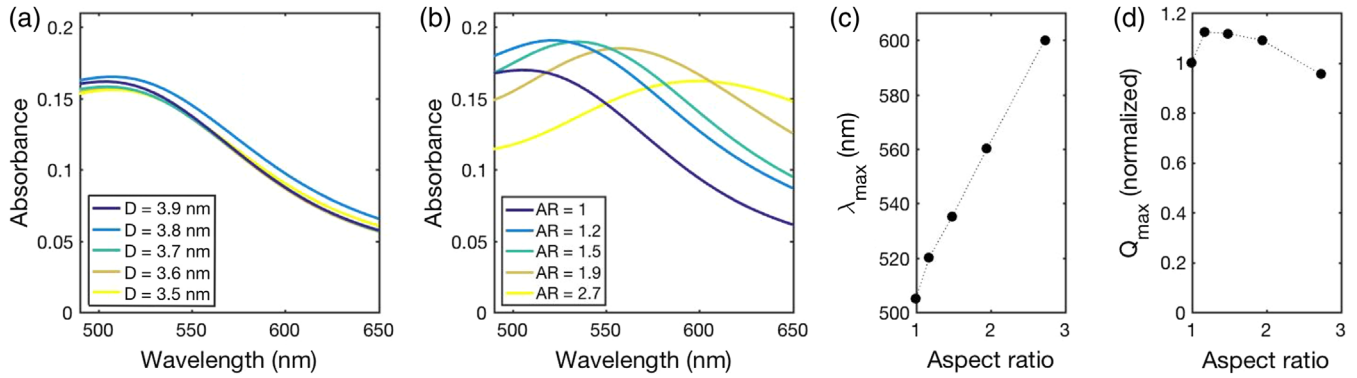

FIG. 4. Simulated optical absorbance. (a) Absorbance of spherical nanocrystals with varying diameter (D). (b) Absorbance of oblate spheroidal nanocrystals with constant volume (equal to sphere with 3.9 nm diameter) and varying aspect ratio (AR). (c) Plasmon peak wavelength (λ_{max}) and (d) absorbance efficiency (Q_{max}) corresponding to (b).

not change significantly when the nanocrystal diameter is changed from 3.9 to 3.5 nm. The diameter of the Au nanocrystals is expected to change by this amount in experiment according to the bulk modulus for a macroscale Au structure [45], although the bulk modulus may be different for a Au nanocrystal [18]. These results indicate that compressional effects, such as changes in bound and free electron density under pressure, are not significant in small Au nanocrystals. The effect of changing electron density is small because free electrons are delocalized outside of the nanocrystal (electron spill-out effect) in nanocrystals with diameters of less than 10 nm and are not strongly affected by lattice contraction [24,46,47]. A previous simulation study observed a redshift of more than 100 nm in 10–100 nm Au nanocrystals under 5% volumetric compression when electron density effects are prominent [46].

The simulated and experimental spectra for Au nanocrystals under quasihydrostatic pressure indicate that a small change in volume has a negligible effect on Au plasmonic properties. Therefore, the effect of volumetric strain can be omitted in regard to the large changes in λ_{max} and Q_{max} under nonhydrostatic pressure, although a small amount of volumetric strain occurs in these tests. The optical spectra of oblate spheroids are simulated to quantify the effects of deviatoric strain on Au nanocrystals under nonhydrostatic pressure [Fig. 4(b)]. Figure 4(b) shows the absorbance spectra of spheroidal Au nanocrystals with aspect ratios (ARs) of 1 to 2.7 (AR is defined as the ratio of the major axis to minor axis of the ellipsoidal cross section of the spheroid), and the volume equal to a 3.9 nm sphere. λ_{max} increases from 505 to 600 nm when aspect ratio is increased from 1 to 2.7 [Fig. 4(c)]. Q_{max} increases to 1.12 arb. units when the aspect ratio is increased to 1.2 due to the changing refractive index environment. Q_{max} decreases with further increases in aspect ratio [Fig. 4(d)]. These results support the conclusion that the experimentally observed redshift under nonhydrostatic pressure is due to nanocrystal shape change.

While the initial increase and subsequent decrease in the simulated Q_{max} is similar to the experiment [Figs. 2(e), 2(f), and 2(h)], the magnitude of the decrease in Q_{max} is larger in the experiment than the simulation. In particular, the large decrease in the experimental Q_{max} that occurs upon decreasing pressure to ambient conditions does not match the simulated change in Q_{max}, and it cannot be attributed to changes in nanocrystal geometry. Previous experiments show that polycrystalline Au and Ag nanocrystals have lower absorbance efficiency (Q_{max}) than single crystal nanocrystals, but similar plasmon wavelength (λ_{max}) [25,26]. By contrast, electrodynamics simulations on crystalline defects in Au nanoshells determined that defects have no influence on optical absorbance [48], while atomistic simulations on Ag nanocubes observed a significant redshift and reduction in absorbance efficiency in sub-3 nm nanocrystals containing planar defects (e.g., partial and full dislocations) [49]. Further studies are required to resolve these conflicting reports. The presence of crystalline defects is modeled in our simulation as an increase in free electron damping (see the Supplemental Material [29]). The density of crystalline defects is increased until equivalent to a Au thin film with a 1.2 nm grain size [50]. This leads to a 10 nm redshift and a 33% decrease in absorbance efficiency. This result indicates that the experimentally observed changes in λ_{max} and Q_{max} are due to a combination of shape change and the emergence of defects.

Using these simulation results, we estimate that the Au nanocrystals experience uniaxial strain of up to 14%–20% in the nonhydrostatic experiments assuming that the Au nanocrystals become oblate spheroids under pressure with aspect ratios of 1.6 to 2. This strain far exceeds the elastic limit for bulk Au. Previous diamond anvil cell experiments on Au and other metals in nonhydrostatic environments show that yield strength increases by ~1 GPa over the pressure range in our experiments [41,42,51]. The uniaxial pressure in our experiments exceeds the pressure-dependent yield stress for Au such that plastic deformation (breaking of atomic bonds) is expected to occur in the

Au nanocrystals. The reversible deformation observed in the Au nanocrystals involves a pseudoelastic transformation in which the Au nanocrystals recover their original shape after atoms within the nanocrystals lose their original coordinates and connectivity. This agrees with the recent observation of pseudoelasticity in sub-10 nm Ag nanocrystals [1], but it is the first time this phenomenon has been observed in an ensemble of nanocrystals, and outside of an electron microscope. Previous diamond anvil cell experiments on ~40 nm colloidal Au nanocrystals at dilute concentrations under nonhydrostatic conditions resulted in irreversible deformation and fracture under pressure [19,20]. Thus, pseudoelasticity is active on experimental timescales (minutes) only in very small Au nanocrystals.

One possible mechanism for pseudoelasticity in small nanocrystals is curvature-driven surface diffusion, as implicated in the recent observation of pseudoelasticity in sub-10 nm Ag nanocrystals [1]. Classical curvature-driven shape equilibration theory predicts equilibration times on the order of seconds for Au nanocrystals with radii of 2 nm (see Supplemental Material [29]) [37], which is well within the timescale of shape recovery observed in this study. However, it does not account for the defects that form in the Au nanocrystals under pressure.

Crystalline defects were not observed during the pseudoelastic deformation of sub-10 nm Ag nanocrystals [1], although there may be dislocations that are invisible at the imaging conditions, or that move too rapidly to be captured by TEM. By contrast, our optical measurements and modeling indicate that crystalline defects form in the interior of the Au nanocrystals during deformation. The mechanism behind the pseudoelasticity in the Au nanocrystals is investigated by compressing nanocrystal samples over two pressure cycles to determine the time and history dependence of the optical response. Figures 5(a) and 5(c) correspond to an experiment in which pressure cycle 2 occurred 30 min after the end of cycle 1. The change in λ_{max} is extremely similar over the two pressure cycles [Fig. 5(a)]. The final λ_{max} is identical to the initial λ_{max} after cycle 1 and is redshifted by 10 nm relative to the initial λ_{max} after cycle 2. The shape of the Q_{max} vs pressure curve is similar for the two cycles [Fig. 3(c)], but the initial absorbance efficiency of cycle 2 is reduced by 0.45 relative to cycle 1. The shape of the Q_{max} vs pressure curve is similar for the two cycles because the change in strain of the diamond anvil cell chamber is very similar for the two cycles (see the Supplemental Material [29]). In the experiment in Figs. 3(b) and 3(d), cycle 2 occurs 15.5 h after cycle 1. Interestingly, the initial Q_{max} at the beginning of the second cycle is significantly greater than the final Q_{max} of the first cycle [Fig. 3(d)], which indicates that there is recovery of absorbance efficiency in this time.

In Fig. 5, the final Q_{max} is always lower than the initial Q_{max} within one pressure cycle. This indicates that structural deformation accumulates during the course of the pressure cycle and can be retained between pressure cycles. The time-dependent changes in Q_{max} between pressure cycles presents an intriguing clue as to the structural changes occurring in the nanocrystals, but they require more careful investigation before conclusions can be made. The post-deformation TEM images of nanocrystals were taken several days after the diamond anvil cell experiments were performed (Fig. 3). Crystalline defects that were initially present in the nanocrystals after deformation may have healed before imaging through dislocation-mediated processes such as escape through free surfaces [52,53]. Direct structural measurements, such as through high-pressure x-ray diffraction, could provide further insights into the mechanism of pseudoelasticity in Au nanocrystals.

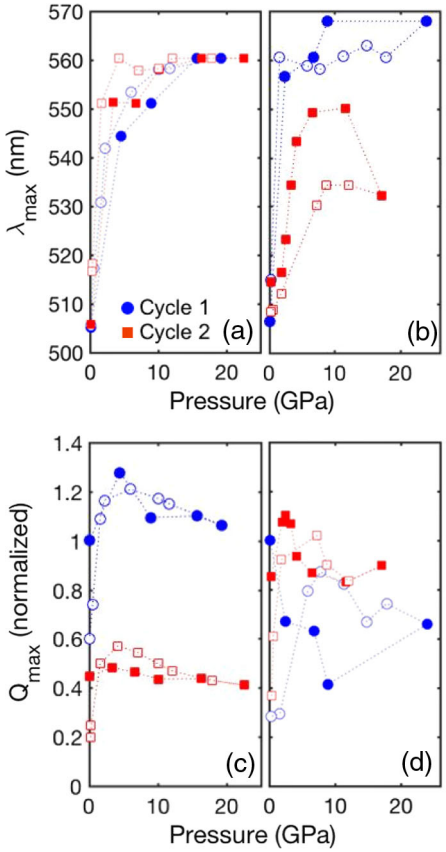

FIG. 5. Multiple nonhydrostatic pressure cycles. (a),(b) The plasmon peak wavelength (λ_{max}) and (c),(d) the corresponding absorbance efficiency (Q_{max}) during cycle 1 (blue) and cycle 2 (red) during two experiments where the cycles are spaced apart by (a),(c) a half hour and (b),(d) 15.5 h. Increasing pressures are filled symbols, and decreasing pressures are open symbols.

In summary, 3.9 nm Au nanocrystals are compressed under quasihydrostatic and nonhydrostatic conditions in a diamond anvil cell. Changes in nanocrystal structure under pressure are monitored using optical absorbance. Nanocrystals under quasihydrostatic pressure do not exhibit a change in plasmon wavelength. Nanocrystals under nonhydrostatic pressure exhibit a reversible redshift

of the plasmon wavelength of up to 68 nm over ~20 GPa. The absorbance efficiency is reduced to 30%–60% of its original value after the nonhydrostatic pressure cycle. Optical modeling was performed to correlate changes in absorbance to strain and lattice disorder in the nanocrystals. The results of this model indicate that the nanocrystals deform up to ~20% strain (equivalent to an aspect ratio of 2) under nonhydrostatic pressure yet are able to recover their original spherical shape. Postcompression TEM images demonstrate that the nanocrystals return to their original shape after the pressure cycle. The Au nanocrystals exhibit room temperature pseudoelastic shape recovery at large strains, which differs completely from bulk scale behavior. A reduction in nanocrystal absorbance efficiency is related to increased free electron scattering due to the presence of crystalline defects. This indicates that the nonhydrostatic deformation of Au nanocrystals likely leads to an increase in the number of defects, such as dislocations in the nanocrystals.

Our discovery of pseudoelasticity in small Au nanocrystals implies that the metallic nanostructures used in nanoscale machines, devices, and patterned surfaces may demonstrate rapid self-healing and resilience against external stresses and strains. The relevance of these findings extends beyond nanofabrication and crystal growth. Au nanocrystals could be used as nanoscale strain gauges that can differentiate between volumetric and deviatoric strains with a reversible, pressure-dependent optical readout that has better sensitivity than existing nanocrystal sensors [17,21,54–56]. It remains to be seen whether pseudoelasticity is universal across different nanoscale metals, and when embedded in a variety of matrices.

We gratefully acknowledge financial support from the U.S. Department of Energy, Office of Science, Office of Basic Energy Sciences, Materials Sciences and Engineering Division, under Contract No. DE-AC02-05CH11231 within the Inorganic or Organic Nanocomposites Program (KC3104). C. N. E. acknowledges support from the Office of Energy Efficiency and Renewable Energy Postdoctoral Fellowship Program (U.S. Department of Energy). We would like to thank Dr. Son Nguyen for help with synthesizing nanocrystals, and Professor Bill Nix, Andy Minor, and Raymond Jeanloz for a critical reading of the manuscript.

*These authors contributed equally to this work.
†Corresponding author.
paul.alivisatos@berkeley.edu

[1] J. Sun, L. He, Y.-C. Lo, T. Xu, H. Bi, L. Sun, Z. Zhang, S. X. Mao, and J. Li, Nat. Mater. **13**, 1007 (2014).
[2] O. Kovalenko, C. Brandl, L. Klinger, and E. Rabkin, Adv. Sci. **4**, 1700159 (2017).
[3] X. Huang, I. H. El-Sayed, W. Qian, and M. A. El-Sayed, J. Am. Chem. Soc. **128**, 2115 (2006).
[4] L. R. Hirsch, R. J. Stafford, J. A. Bankson, S. R. Sershen, B. Rivera, R. E. Price, J. D. Hazle, N. J. Halas, and J. L. West, Proc. Natl. Acad. Sci. U.S.A. **100**, 13549 (2003).
[5] W. Liang, M. Zhou, and F. Ke, Nano Lett. **5**, 2039 (2005).
[6] J. Wang, Z. Zeng, C. R. Weinberger, Z. Zhang, T. Zhu, and S. X. Mao, Nat. Mater. **14**, 594 (2015).
[7] W. L. Barnes, A. Dereux, and T. W. Ebbesen, Nature (London) **424**, 824 (2003).
[8] S. Lal, S. Link, and N. J. Halas, Nat. Photonics **1**, 641 (2007).
[9] P. V. Kamat, J. Phys. Chem. B **106**, 7729 (2002).
[10] J. Zeng, Q. Zhang, J. Chen, and Y. Xia, Nano Lett. **10**, 30 (2010).
[11] C. Sönnichsen, B. M. Reinhard, J. Liphardt, and A. P. Alivisatos, Nat. Biotechnol. **23**, 741 (2005).
[12] K. A. Willets and R. P. Van Duyne Annu. Rev. Phys. Chem. **58**, 267 (2007).
[13] X. Xia, S. Xie, M. Liu, H.-C. Peng, N. Lu, J. Wang, M. J. Kim, and Y. Xia, Proc. Natl. Acad. Sci. U.S.A. **110**, 6669 (2013).
[14] Y. Lu, J. Y. Huang, C. Wang, S. Sun, and J. Lou, Nat. Nanotechnol. **5**, 218 (2010).
[15] S. Y. Kim, I.-H. Lee, and S. Jun, Phys. Rev. B **76**, 245407 (2007).
[16] S. H. Tolbert and A. P. Alivisatos, Science **265**, 373 (1994).
[17] C. L. Choi, K. J. Koski, S. Sivasankar, and A. P. Alivisatos, Nano Lett. **9**, 3544 (2009).
[18] Q. F. Gu, G. Krauss, W. Steurer, F. Gramm, and A. Cervellino, Phys. Rev. Lett. **100**, 045502 (2008).
[19] Y. Bao, B. Zhao, D. Hou, J. Liu, F. Wang, X. Wang, and T. Cui, J. Appl. Phys. **115**, 223503 (2014).
[20] Y. Bao, B. Zhao, X. Tang, D. Hou, J. Cai, S. Tang, J. Liu, F. Wang, and T. Cui, Appl. Phys. Lett. **107**, 201909 (2015).
[21] A. Lay, D. S. Wang, M. D. Wisser, R. D. Mehlenbacher, Y. Lin, M. B. Goodman, W. L. Mao, and J. A. Dionne, Nano Lett. **17**, 4172 (2017).
[22] K. Lance Kelly, E. Coronado, L. Lin Zhao, and G. C. Schatz, J. Phys. Chem. B **107**, 668 (2003).
[23] S. Link and M. A. El-Sayed, J. Phys. Chem. B **103**, 8410 (1999).
[24] G. V. Hartland, Chem. Rev. **111**, 3858 (2011).
[25] N. Goubet, C. Yan, D. Polli, H. Portalès, I. Arfaoui, G. Cerullo, and M.-P. Pileni, Nano Lett. **13**, 504 (2013).
[26] Tanvi, A. Mahajan, R. K. Bedi, S. Kumar, V. Saxena, and D. K. Aswal, J. Appl. Phys. **117**, 083111 (2015).
[27] S. Peng, Y. Lee, C. Wang, H. Yin, S. Dai, and S. Sun, Nano Res. **1**, 229 (2008).
[28] C. Herbst, R. Cook, and H. King, J. Non-Cryst. Solids **172–174**, 265 (1994).
[29] See Supplemental Material at http://link.aps.org/supplemental/10.1103/PhysRevLett.121.056102, which includes Refs. [30–39], for methods, details of optical and strain analysis, optical modeling, additional postcompression TEM images, and calculations.
[30] H. K. Mao, J. Xu, and P. M. Bell, J. Geophys. Res. **91**, 4673 (1986).
[31] J. Van Straaten, R. J. Wijngaarden, and I. F. Silvera, Phys. Rev. Lett. **48**, 97 (1982).

[32] J. Van Straaten and I. F. Silvera, Phys. Rev. B **37**, 6478 (1988).
[33] L. B. Scaffardi and J. O. Tocho, Nanotechnology **17**, 1309 (2006).
[34] E. A. Coronado and G. C. Schatz, J. Chem. Phys. **119**, 3926 (2003).
[35] U. Kreibig, Z. Phys. B **31**, 39 (1978).
[36] U. Kreibig and L. Genzel, Surf. Sci. **156**, 678 (1985).
[37] F. A. Nichols and W. W. Mullins, AIME Trans. **233**, 1840 (1965).
[38] D. Holec, P. Dumitraschkewitz, F. D. Fischer, and D. Vollath, arXiv:1412.7195.
[39] H. Göbel and P. von Blanckenhagen, Surf. Sci. **331-333**, 885 (1995).
[40] T. S. Duffy, G. Shen, D. L. Heinz, J. Shu, Y. Ma, H.-K. Mao, R. J. Hemley, and A. K. Singh, Phys. Rev. B **60**, 15063 (1999).
[41] A. K. Singh, H.-P. Liermann, Y. Akahama, S. K. Saxena, and E. Menéndez-Proupin, J. Appl. Phys. **103**, 063524 (2008).
[42] A. K. Singh, H. P. Liermann, S. K. Saxena, H. K. Mao, and S. U. Devi, J. Phys. Condens. Matter **18**, S969 (2006).
[43] C. B. Murray, C. R. Kagan, and M. G. Bawendi, Annu. Rev. Mater. Sci. **30**, 545 (2000).
[44] M. P. Pileni, J. Phys. Chem. B **105**, 3358 (2001).
[45] F. Cardarelli, *Materials Handbook* (Springer, London, 2008).
[46] X. Qian and H. S. Park, J. Mech. Phys. Solids **58**, 330 (2010).
[47] C. Voisin, D. Christofilos, P. A. Loukakos, N. Del Fatti, F. Vallée, J. Lermé, M. Gaudry, E. Cottancin, M. Pellarin, and M. Broyer, Phys. Rev. B **69**, 195416 (2004).
[48] E. Hao, S. Li, R. C. Bailey, S. Zou, G. C. Schatz, and J. T. Hupp, J. Phys. Chem. B **108**, 1224 (2004).
[49] X. Ben, P. Cao, and H. S. Park, J. Phys. Chem. C **117**, 13738 (2013).
[50] D. I. Yakubovsky, A. V. Arsenin, Y. V. Stebunov, D. Y. Fedyanin, and V. S. Volkov, Opt. Express **25**, 25574 (2017).
[51] R. J. Hemley, H. Mao, G. Shen, J. Badro, P. Gillet, M. Hanfland, and D. Häusermann, Science **276**, 1242 (1997).
[52] D. Mordehai, E. Rabkin, and D. J. Srolovitz, Phys. Rev. Lett. **107**, 096101 (2011).
[53] R. Kositski and D. Mordehai, Acta Mater. **136**, 190 (2017).
[54] C. L. Choi, K. J. Koski, A. C. K. Olson, and A. P. Alivisatos, Proc. Natl. Acad. Sci. U.S.A. **107**, 21306 (2010).
[55] A. Stevenson, A. Jones, and S. Raghavan, Nano Lett. **11**, 3274 (2011).
[56] X. Jin, M. Götz, S. Wille, Y. K. Mishra, R. Adelung, and C. Zollfrank, Adv. Mater. **25**, 1342 (2013).